THE JOURNAL OF PHYSICAL CHEMISTRY C
A JOURNAL OF THE AMERICAN CHEMICAL SOCIETY

pubs.acs.org/JPCC

Article

Field-Dependent Orientation and Free Energy of D_2O at an Electrode Surface Observed via SFG Spectroscopy

Published as part of The Journal of Physical Chemistry virtual special issue "Honoring Michael R. Berman".

Angelo Montenegro, Ariel E. Vaughn, Muhammet Mammetkuliyev, Bofan Zhao, Boxin Zhang, Haotian Shi, Dhritiman Bhattacharyya, Alexander V. Benderskii, and Stephen B. Cronin*

Cite This: https://doi.org/10.1021/acs.jpcc.2c06063

Read Online

ACCESS | Metrics & More | Article Recommendations | Supporting Information

ABSTRACT: Polarization-selected vibrational sum frequency generation (SFG) spectroscopy of D_2O is used to obtain the orientation of the free OD bond at a monolayer graphene electrode. We modulate the interfacial field by varying the applied electrochemical potential, and we measure the resulting change in the orientation. A hyperpolarizability model is used for the orientational analysis, which assumes a quadratic free energy orienting potential in the absence of the field, whose minimum and curvature determine the average tilt angle and the Gaussian width of the orientational distribution. The average free OD tilt angle changes in an approximately linear fashion with the applied field, from 46° from normal at −0.9 V vs Ag/AgCl (E = −0.02 V/Å) to 32° at −3.9 V vs Ag/AgCl (E = −0.17 V/Å). Using this approach, we map the free energy profile for the molecular orientation of interfacial water by measuring the reversible response to an external perturbation, i.e., a torque applied by an electric field acting on the molecule's permanent dipole moment. This allows us to extract the curvature of the free energy orienting potential of interfacial water, which is (4.0 ± 0.8) × 10^{-20} J/rad^2 (or 0.25 ± 0.05 eV/rad^2).

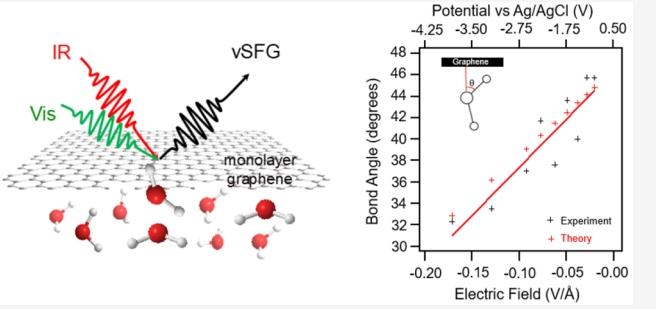

INTRODUCTION

The free energy potential is one of the most useful concepts in statistical mechanics, allowing one to keep track of both enthalpic and entropic contributions averaged over the molecular dynamics of thermal motion. It allows one to predict both the equilibrium properties and fluctuations as well as physical/chemical transformation rates and equilibrium constants. However, only the free energy differences between the initial and final states have been readily accessible experimentally, while the free energy profile (also known as the potential of mean force, PMF) has been mostly a theoretical construct, calculated, e.g., using molecular dynamics (MD) computer simulations. Only recently, for single-molecule experiments, the inversion of the free energy potential from force-pulling experiments has become possible by using the Jarzynski equality, a nonequilibrium extension of the reversible work theorem.[1,2] X-ray reflectivity measurements of electrified liquid interfaces have also been interpreted in terms of the potential of mean force for the spatial distribution of ions.[3] Here, we present a strategy for experimentally probing the free energy profile for molecular reorientation from an ensemble-averaged measurement by measuring the reversible response of a system to an external perturbation, a torque applied by an electric field acting on the molecule's permanent dipole moment.

The behavior of water at charged interfaces plays an important role in a variety of chemical and biological process ranging from electrocatalysis to biomembranes.[4−7] Through the use of surfactants, the orientation of water at charged interfaces has been studied extensively using vibrational sum frequency generation (SFG) spectroscopy.[7−11] SFG is a second-order nonlinear optical process based on the annihilation of two input photons at angular frequencies ω_1 and ω_2 while, simultaneously, one photon at frequency ω_3 is generated.[12] As with any second-order $\chi^{(2)}$ phenomenon in nonlinear optics, this can only occur under conditions where the light is interacting with matter that is asymmetric (e.g., surfaces and interfaces) and the light has a very high intensity (i.e., pulsed laser), thus providing highly surface selective spectroscopy. SFG is a *parametric process*, with photons

Received: August 24, 2022
Revised: October 30, 2022

satisfying energy conservation, leaving the matter unchanged after the interaction: $\hbar\omega_1 + \hbar\omega_2 = \hbar\omega_3$.These previous SFG studies[7−11] require either multiple experiments or changing the pH of the solution to modify the charged interface, making the process more difficult to interpret and calling into question the effects of other parameters such as ions in the solutions. Using electrodes, the ordering of water has been studied at different voltages using X-ray scattering.[6] To the authors' knowledge, the orientation of water as a function applied voltage has not been previously reported.

In the vibrational spectra of water, there are typically two peaks associated with the OH stretch mode around 3200−3500 cm^{-1}, which are significantly broadened due to hydrogen bonding in the bulk water solution. SFG spectroscopy is a surface-sensitive spectroscopy that uses the nonlinear optical mixing of visible and IR beams to measure the vibrational spectra of molecules at an interface. In 1993, Du et al. reported SFG spectra observed at the air/water interface, which exhibited a "free−OH" mode (i.e., projecting up into the air) at 3700 cm^{-1}.[13−15] Because this free OH bond is projecting up away from the bulk water and is therefore not hydrogen bonded, it appears blue-shifted and is relatively narrow compared to the hydrogen-bonded OH modes. Ohno et al. used SFG spectroscopy to explore the second-order vibrational line shapes of the air/water interfaces, presenting an analysis of nonlinear optical spectra obtained from charged air/water and solid/liquid interfaces, demonstrating the importance of the interfacial potential-dependent $\chi^{(3)}$ term in interpreting line shapes when seeking molecular information from charged interfaces using second-order spectroscopy.[16,17] Most of the previous SFG measurements on interfacial water entailed static experiments.[7−11] AlSalem et al. reported SFG spectra of phenyl groups on graphene, although not in an electrolyte.[18] Peng et al. performed *in situ* SFG spectra of Li redox reactions at a graphene electrode; however, no water spectra were reported.[19] The wettability of graphene was investigated by Kim et al. using SFG; however, no potential was applied.[20] Dreier et al. explored the pH and potential dependence of the interfacial water structure in contact with graphene using SFG. However, their spectra do not show any clear signatures of the free OD feature at the graphene−D_2O interface.[21] More recently, Montenegro et al. measured *in situ* SFG spectra of water at a water/graphene interface under applied electrochemical potentials.[22] They observed the emergence of a free OD peak under large negative (i.e., reducing) potentials and complete suppression of the hydrogen-bonded OD peaks. In the work presented here, we extend this study to even larger negative potentials and perform polarization-selective SFG spectra to extract the average OD bond angles as a function of the applied potential.[23,24]

Several groups have calculated the SFG spectra of water at water/graphene interfaces. Zhang et al. calculated SFG spectra of water at electrified graphene interfaces using classical molecular dynamics simulations.[25,26] However, they predict a free OH peak that is largely potential independent and a hydrogen-bonded region that increases in intensity at increasingly reducing potentials (i.e., more negative potentials), which stands in contrast to our previous experimental observations.[22] Ohto et al. also simulated SFG spectra of water at water/graphene interfaces using *ab initio* molecular dynamics simulations and found a sharp free OD peak around 2645 cm^{-1}, indicating that the graphene is hydrophobic.[27] In yet another molecular dynamics study of the graphene/water interface, Eaves and Ostrowski predict hydrophobicity under both positively (p-doped) and negatively (n-doped) charged graphene, resulting in a 3 Å gap between graphene and water.[28] An experimental observation of the angular dependence of water molecules as a function of applied electric field could be directly compared with theoretical calculations providing a way to validate and improve future models of water.

METHODS AND MATERIALS

Graphene Electrode Preparation. A 1 cm × 1.5 cm strip of monolayer graphene was grown by chemical vapor deposition (CVD) on copper foil and transferred onto a CaF_2 window (1 in. diameter × 2 mm) for support.[29−31] Prior to transfer, two strips of gold (50 nm thick) were deposited onto the CaF_2 window. The two gold strips are in electrical contact with the graphene strip, which bridges the gap between them. The gold strips provide macroscopic contacts through which voltage is applied to the graphene (Figure 1), and the in-plane resistance of graphene is monitored periodically (typically 1−2 kΩ). A permanent 3-fold increase (or more) in the in-plane resistance roughly correlated to degradation of the graphene monolayer.

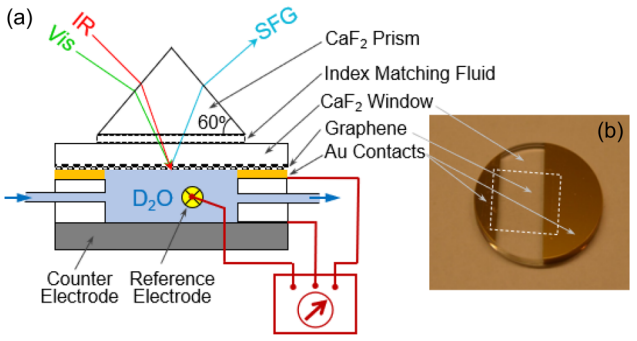

Figure 1. (a) Schematic diagram of the prism, index-matching fluid, CaF_2 window, and graphene electrode, which are nearly transparent to the IR, visible, and SFG beams. The cell is shown in the three-terminal configuration; graphene, the Ag/AgCl reference electrode, and the glassy carbon counter electrode are connected to a potentiostat. In the two-terminal configuration, the Ag/AgCl reference electrode is absent; graphene and glassy carbon electrodes are connected to a two-terminal voltage source. (b) Photograph of the graphene electrode (labels in gray), which is inverted so that graphene faces D_2O when placed in the electrochemical flow cell.

Electrochemical Cell. The CaF_2-supported graphene electrode serves as the top window of the electrochemical flow cell (Figure 1) and is transparent to all wavelengths of interest in this study. The CaF_2 prism enhances the SFG signal significantly via total internal reflection.[32] The small gap between the prism and the CaF_2 window was filled with index matching fluid (dimethylformamide). The graphene (working electrode; top) and glassy carbon (counter electrode; bottom) electrodes are separated by a hollow, cylindrically shaped Teflon spacer. The graphene electrode is inverted, such that it is adjacent to D_2O, which continually flows through the Teflon spacer to reduce laser-induced heating of the graphene electrode.

For measurements performed in a two-terminal configuration, the graphene and glassy carbon electrodes are connected to the positive and negative terminals of a voltage source, respectively (Keithley Instruments, Model 2400). In

https://doi.org/10.1021/acs.jpcc.2c06063
J. Phys. Chem. C XXXX, XXX, XXX−XXX

the three-terminal configuration, an Ag/AgCl reference electrode was inserted through the side wall of the Teflon spacer. The working, counter, and reference electrodes were connected to a potentiostat (Gamry Instruments, Reference 600). To keep the water pure, it is maintained in a purged atmosphere, eliminating CO_2 using a purge-gas generator (Parker Balston, Model 75-62).

Vibrational Sum Frequency Generation Setup. A femtosecond (100 fs) broadband pulse centered at 2700 cm^{-1} (FWHM = 300 cm^{-1}) excites the free OD stretching vibration at the graphene−water interface, inducing a first-order polarization. The first-order polarization is upconverted to a second-order polarization via a picosecond narrow-band visible (800 nm) pulse, yielding an SFG signal that propagates in the phase-matched direction. The signal was dispersed onto a liquid nitrogen cooled charged-coupled device (CCD) array detector (Roeper Scientific, Spec-10:100B, 1340 × 100 pixels) using a single-grating monochromator (Princeton Instruments Acton SP2500). The IR and visible beams copropagate in the plane of incidence with an angle of 60° and 68° with respect to the surface normal. Spot sizes were focused to 200 μm (IR) and 250 μm (vis) at the graphene−water interface. The average powers were 12 mW (IR) and 25 mW (vis). The 60° equilateral CaF_2 prism significantly enhances the VSFG signal.[32] The small gap between the prism and the CaF_2 window was filled with index matching fluid (dimethylformamide). The raw VSFG spectra were background subtracted and normalized by the nonresonant PPP spectrum of gold.

This optical approach includes several improvements over that used our previous work.[22] Introducing a CaF_2 prism increased our signal-to-noise ratio by several orders of magnitude via total internal reflection, and collecting spectra over a shorter wavelength range allowed us to increase IR power and, ultimately, measure much weaker signals, with much shorter acquisition times. These improvements reduced our spectral acquisition times from approximately 15 to 1 min, enabling us to collect data at substantially lower potentials than our previous work. Also, using triple-distilled DI water for the transfer of monolayer graphene to CaF_2 increased the low-potential robustness of this electrode, further enabling our ability to collect spectra at low potentials (i.e., −3.9 V vs Ag/AgCl (E = −0.17 V/Å)).

Raman Experimental Setup. Voltage-dependent Raman spectra of the graphene electrode's G band (∼1585 cm^{-1}) were collected using a Renishaw micro-Raman spectrometer in both the two-terminal and three-terminal configurations. The G band Raman shift ($\Delta\omega_G$) responds linearly to the excess charge density, as follows:[33,34]

$$\text{electrons:}\quad E_f = 21\Delta\omega_G + 75\ [\text{cm}^{-1}] \tag{1}$$

$$\text{holes:}\quad E_f = -18\Delta\omega_G - 83\ [\text{cm}^{-1}] \tag{2}$$

$$n = \left(\frac{E_f}{11.65}\right)^2 10^{10}\ [\text{cm}^{-2}] \tag{3}$$

Thus, the G band shift provides a direct measure of the surface charge density (σ) that can be correlated to the applied two- and three-terminal voltages. The magnitude of the applied field at the interface, E, was estimated by treating the graphene electrode as an infinite plane of charge that is separated from water by an ∼3 Å gap.[27,28]

$$E = \frac{\sigma}{2\varepsilon_0\varepsilon} \quad (\text{with } \varepsilon = 1) \tag{4}$$

Measurements were conducted using a backscattering geometry with a 50 μW, linearly polarized 532 nm laser beam focused to a 1 μm diameter. The collected Raman scattered light was dispersed onto a charged-coupled device (CCD) array detector by a single-grating monochromator with a spectral resolution of approximately 0.5 cm^{-1}.

RESULTS

Figure 1a shows a schematic diagram of our experimental setup, which takes advantage of total internal reflection using a prism and calcium fluoride window mounted on the top of an electrochemical flow cell. A monolayer graphene electrode is mounted on the bottom surface of the calcium fluoride window (Figure 1b) through which SFG spectra are collected. This "flipped" geometry avoids intensity loss and spectral distortion of the IR beam due to the strong absorption of water. The inert surface of the graphene electrode allows us to explore a remarkably broad range of electrochemical potentials, from +1.5 to −3.9 V vs Ag/AgCl, without any significant redox currents and chemical reactions at the surface. Further experimental details are given in the Methods and Materials section.

Figure 1c shows representative vibrational SFG spectra taken at three different electrode potentials. Spectra taken above −1.0 V vs Ag/AgCl (i.e., 0 and +1 V spectra shown in the figure) display two broad peaks between 2300 and 2600 cm^{-1} corresponding to the hydrogen-bonded OD stretch mode.[21,22,27] The application of a sufficiently negative potential, below −1.0 V vs Ag/AgCl, leads to the sudden onset of a narrow and spectrally isolated peak in the SFG spectra around 2690 cm^{-1} assigned to a local OD stretch vibration that is not hydrogen bonded (i.e., the "free OD")[14,35] and near complete suppression of the hydrogen-bonded peaks.[22] The SFG signal is inherently dependent on incoming angles.[36] The use of a prism further suppresses the hydrogen-bonded peaks due to changes in the Fresnel factors. This results in the amplification of only the free OD signal, allowing for detection over a larger voltage range than in our previous work.[22] The free OD species are believed to exist in the topmost monolayer adjacent to graphene (at the air/water interface, they comprise approximately 25% of the first monolayer). Because of its hydrophobic nature, the existence of a 3 Å gap has been predicted between the graphene and the water by MD simulations.[27,28] This "free" OD (or OH) species is absent at most charged interfaces (e.g., surfactants with charged headgroups and mineral surfaces) because water tends to form hydrogen bonds with these interfaces. Unlike the hydrogen-bonded spectral features that represent vibrations delocalized over as many as 10 water molecules and are strongly influenced by vibrational excitonic coupling effects,[37] the free OD vibrational mode is local and not coupled to the other OD oscillators in the system[35] and thus renders itself to a rigorous spectroscopic and orientational analysis. In what follows, we investigate the evolution of this feature while varying the applied electrode potential.

A tunable DC electric field is generated at the interface by applying an electrochemical potential, which dopes the graphene electrode with excess charge. We used the frequency shift of the graphene Raman G band to calibrate the electron doping levels at negative applied potentials (Figure S1).[22] This

https://doi.org/10.1021/acs.jpcc.2c06063
J. Phys. Chem. C XXXX, XXX, XXX−XXX

allows us to calculate the strength of the applied DC electric field, $E = \frac{\sigma}{2\varepsilon_0\varepsilon}$. In our analysis, we assume that the free OD groups, which point into the water−graphene gap, experience the applied field with $\varepsilon = 1$. This gives the range of applied electric field strengths between −0.02 and −0.17 V/Å for the range of applied potentials −0.9 to −3.9 V vs Ag/AgCl (Figure S2). Note that the potential of zero charge for graphene/water is around +0.15 V vs Ag/AgCl.[22]

Figure 2 shows the electric-field-dependent vibrational SFG spectra of the free OD peak at the graphene/water (D_2O) interface collected in the SSP and PPP polarization configurations. The solid lines are fits to the Lorentzian line shape (see the Methods section). The fitting parameters (amplitudes, central frequencies, and Lorentzian line widths) are collected in Tables S2−S10 of the Supporting Information. The amplitudes in these spectra (shown Figure 3a) show a monotonic increase with the applied electric field magnitude, and the PPP:SSP amplitude ratio increases for stronger negative fields. Qualitatively, this indicates that the free OD bond reorients closer to the surface normal as the deuterium of the free OD is pulled more strongly toward the negatively charged graphene surface (Figure 2c). No free OD peaks were observed at −0.5 V vs Ag/AgCl (and above). The case of PPP:SSP ratio = 1 corresponds to an orientation of approximately 45°. For PPP:SSP ratios less than 1, the angles are greater than 45°. The full details of the orientational analysis and the procedure for extracting the free energy potential surface are described below.

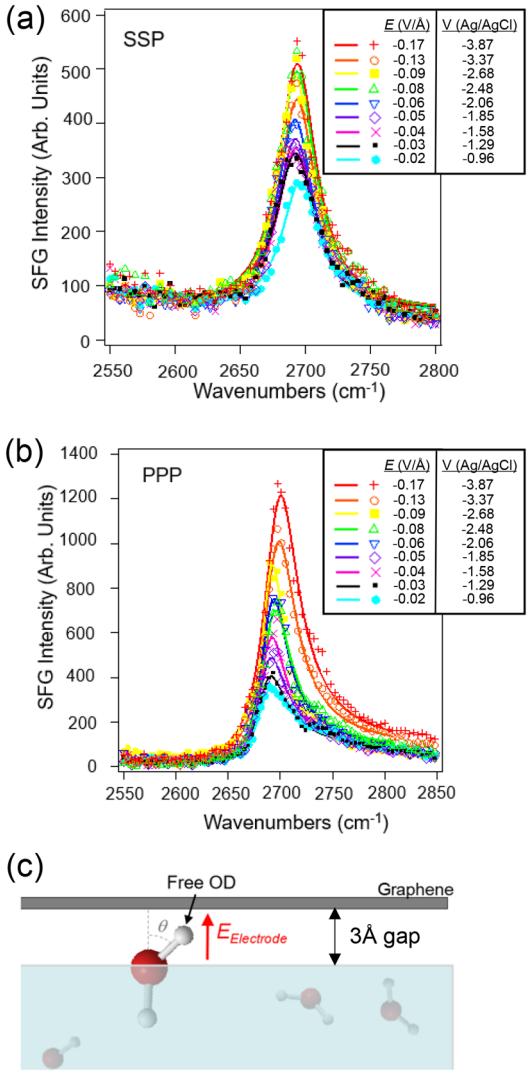

Figure 2. Electric-field-dependent SFG spectra of the graphene−D_2O interface collected in the (a) SSP configuration and (b) PPP configuration. The amplitudes generally increase linearly with the applied electric field strength. (c) Schematic diagram illustrating the topmost OD bond, which rotates up out of the bulk solution under the presence of an electric field and, therefore, is not hydrogen bonded.

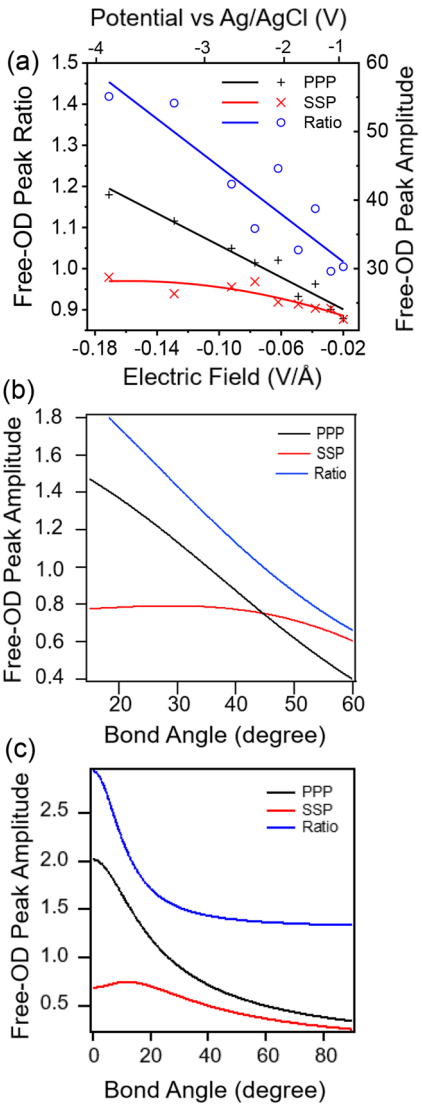

Figure 3. (a) Experimental PPP (black) and SSP (red) amplitudes and their ratio (blue) for a (b) Gaussian distribution of orientation angles with a width of σ = 15° and (c) a decaying exponential distribution of orientation angles. The lines in (a) are linear, and polynomial fits are provided as guides to the eye. The experimental amplitude ratio of PPP to SSP ranges from about 1.0 to 1.4, which are values that do not exist in the calculated blue curve in (c). Thus, the distribution of free OD angles at the graphene−water interface is not well described by a decaying exponential.

https://doi.org/10.1021/acs.jpcc.2c06063
J. Phys. Chem. C XXXX, XXX, XXX−XXX

DISCUSSION

The SFG orientational analysis entails calculation of the ensemble-averaged effective susceptibilities for the PPP and SSP polarization combinations by integration of the product of the three Euler matrices (for the IR, visible, and SFG transition dipoles) over the molecular orientational distribution.[38−40] It requires the knowledge of the molecular hyperpolarizability tensor $\beta^{(2)}_{abc}$ and an assumption of the orientational probability distribution function. The details and equations, including the experimental geometry and the Fresnel coefficients used for the calculations, are presented in the Methods section and in the Supporting Information.

This observation of the free OD species at the graphene−water interface allows an unambiguous and quantitative orientational analysis to be performed because this local vibrational mode is uncoupled from other OD oscillators in the system[35] and has a well-defined direction of the transition dipole along the OD bond. For our analysis, we use the hyperpolarizability tensor elements calculated by Nihonyanagi and co-workers[11] for the free OD mode, $\beta^{(2)}_{aac} = \beta^{(2)}_{bbc} = 0.26$ and $\beta^{(2)}_{ccc} = 1$, which are consistent with a range of 0.23−0.28 that has been reported based on the experimental measurements.[41]

For the orientational distribution of the tilt angle θ of the free OD relative to the surface normal, we have tried a Gaussian probability distribution function $P_0(\theta)$ corresponding to the quadratic free energy potential $\Phi_0(\theta)$ in the absence of the field

$$\Phi_0(\theta) = \frac{1}{2}\kappa(\theta - \theta_0)^2 \tag{5}$$

$$P_0(\theta) = \frac{1}{Z}\exp\left(-\frac{\Phi_0(\theta)}{k_B T}\right) = \frac{1}{Z}\exp\left(-\frac{\kappa(\theta-\theta_0)^2}{2k_B T}\right) = \frac{1}{Z}\exp\left(-\frac{(\theta-\theta_0)^2}{2\sigma_0^2}\right) \tag{6}$$

with the Gaussian width

$$\sigma_0 = \sqrt{\frac{k_B T}{\kappa}} \tag{7}$$

and Z is the partition function (with normalization condition $\int_0^\pi P(\theta)\sin\theta\, d\theta = 1$).

Because there have been suggestions in the literature, based on MD simulations, that the water orientational distribution is exponential,[42−44] we have also tried an exponential function

$$P_0(\theta) = \frac{1}{Z}\exp\left(-\frac{\theta}{\theta_e}\right) \tag{8}$$

albeit corresponding to a somewhat unphysical assumption of a linear orientational free energy $\Phi_0(\theta) = \frac{k_B T}{\theta_e}\theta$.

The calculated PPP and SSP amplitudes (and their ratio) are plotted in Figure 3. For the Gaussian distribution (2), Figure 3b shows the PPP and SSP amplitudes and ratio plotted as a function of the minimum (mean angle) θ_0 for a fixed width σ = 15° (calculations for other values of σ are presented in the Supporting Information; *vide infra*). For the exponential distribution (4), we show the dependence on the parameter θ_e. The experimentally determined PPP and SSP amplitudes and their ratio are shown in Figure 3a. As can be clearly seen, the exponential distribution does not reproduce the experimentally observed range of the PPP/SSP ratios (from 1.0 to 1.4) and can therefore be ruled out. On the contrary, the Gaussian distribution faithfully represents the changes in the amplitudes consistent with the range of tilt angles from ∼45° to ∼30°. We note that the Gaussian model reproduces not only the ratio but also the PPP and SSP amplitudes individually. This suggests that the reorientation, and not the population change of the free OD species, is the main reason for the observed field dependence of the SFG amplitudes, in the range of applied potentials (−0.9 to −3.9 V vs Ag/AgCl). The quantitative correlation between the experimental field dependence of the SFG amplitudes (Figure 3a) and the calculated amplitudes as a function of the free OD tilt angle (Figure 3b) allows us to plot the free OD orientation as a function of the applied electric field, as shown in Figure 4a.

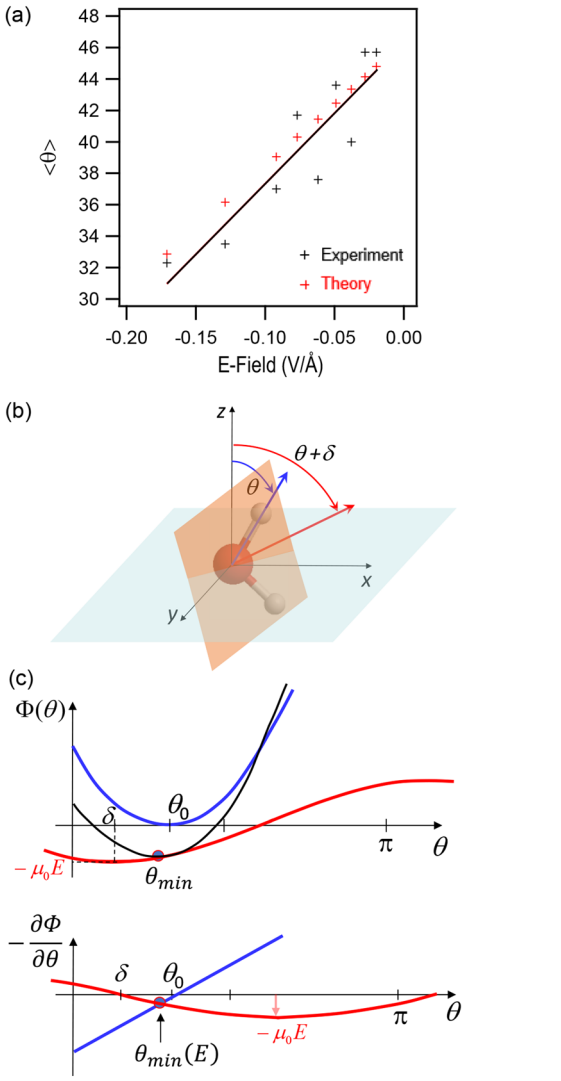

Figure 4. (a) Experimental and calculated free OD bond angle plotted as a function of the applied electric field. The black line corresponds to a linear fit of the experimental data. (b) Illustration of the difference, δ, between the free OD tilt angle (θ) and the orientation of the molecule's permanent dipole. (c) Calculated free energy potential curves, $\Phi(\theta,E)$ and its derivative, where the observed shift to steeper angles with respect to the surface normal is modeled solely through the applied field (E). This reorientation mechanism accounts for a shift in orientation angle from about 46° to 32°.

https://doi.org/10.1021/acs.jpcc.2c06063
J. Phys. Chem. C XXXX, XXX, XXX−XXX

The mean tilt angle $\langle\theta\rangle$ of the free OD changes from 45° with respect to surface normal at E = −0.02 V/Å to 32° at E = −0.17 V/Å. The approximate linearity of the tilt angle variation with the external field is consistent with the assumption of the Gaussian orientational distribution (quadratic free energy potential), as shall be seen below. Error bars for the experimentally determined free OD amplitudes and ratios are given in Tables S2−S10 and lie around 1−2% of the values plotted in Figure 3a.

To provide a phenomenological model of this system, we can describe the behavior of water molecules by adding an additional term in the free energy, a torque of the electric field $\vec{E}$ acting on the molecule's permanent dipole moment μ_0:

$$\Phi(\theta, E) = \Phi_0(\theta) - \vec{\mu}_0 \cdot \vec{E} = \frac{1}{2}\kappa(\theta - \theta_0)^2 \mu_0 E \cos(\theta + \delta) \tag{9}$$

which leads to changes in the orientational probability distribution manifested in the SFG spectral amplitudes (Figure 3b). Here, δ is the difference between the free OD tilt angle (with respect to the surface normal) and the orientation of the molecule's permanent dipole $\vec{\mu}_0$, approximately directed along the C_{2v} symmetry axis (Figure 4). While water molecules do not behave exactly like point dipoles at interfaces, and the local field experienced by a water molecule is different from the applied field, this simple equation provides a basic phenomenological model to understand the general behavior. The maximum possible value of δ is 52.25° (half of the D−O−D angle), corresponding to the case of the plane of the D_2O molecule (orange shade in Figure 4b) perpendicular to the surface plane (teal shade). In reality, however, δ results from averaging of the D_2O molecule's twist angle (around the C_{2v} axis), a value between 0° and 52.25°. As we shall see below, this offset does not yield a large uncertainty in the extracted free energy potential.

Calculating the minimum θ_{min} of this modified free energy (which approximately corresponds to the mean tilt angle $\langle\theta\rangle$, Figure 4c) yields

$$\left.\frac{\partial\Phi(\theta, E)}{\partial\theta}\right|_{\theta_{min}} = \kappa(\theta_{min} - \theta_0) + \mu_0 E \sin(\theta_{min} + \delta) = 0 \tag{10}$$

and for small changes in the tilt angle (weak perturbation by the external field E), we obtain to the first order in the external field

$$\theta_{min}(E) \approx \theta_0 - \frac{\mu_0 \sin(\theta_0 + \delta)}{\kappa} E \tag{11}$$

This is consistent with the experimentally observed linear dependence of the mean tilt angle on the applied field (Figure 4a). It can be easily verified that for our range of applied fields the small parameter in our expansion $\frac{\mu_0 E}{\kappa}$ is of the order of 1/20, and the second-order correction amounts to less than a 1° additional change in the tilt angle, which is within the experimental noise. It can also be seen that the change in the curvature near the bottom of the free energy potential, i.e., the width of the distribution, is also linear in the applied field E:

$$\sigma(E) \approx \sigma_0\left(1 - \frac{\mu_0 E}{2\kappa}\right) \tag{12}$$

Thus, although the distribution narrows toward the surface normal as the applied field gets stronger, it remains approximately Gaussian, and the width change is within the experimental noise level, ±2°. This validates our use of the correlation between the mean tilt angle within the Gaussian distribution of constant width and the calculated SFG amplitudes (Figure 3b) to obtain the free OD orientation as a function of applied field (Figure 4a).

From eq 7 it can be seen that for the physically reasonable range of the offset angle δ, 10°−50°, the factor $\sin(\theta_0 + \delta)$ ranges between 0.82 and 0.99, yielding a possible uncertainty in the extracted force constant κ of 18%. Another possible source of uncertainty is the value of the permanent dipole moment μ_0: for the free OD molecule at the interface, it can range from the gas-phase value of 1.85 to ∼2.5 D in bulk water. The dipole moment error has an upper limit of 35%. However, we believe that the true value is close to the gas-phase value for μ_0, and the error from this assumption is relatively small. Nevertheless, the numbers below can be easily modified if a more accurate or reliable estimate of μ_0 becomes available.

Within the quadratic model of the free energy potential described above, eqs 1 and 5, a self-consistent quantitative interpretation of the SFG data is possible. The calculated PPP and SSP amplitudes (and their ratio) depend on *both* the assumed mean angle $\langle\theta\rangle \approx \theta_{min}$ *and* the Gaussian distribution width σ. We calculated the PPP/SSP ratio as a function of θ_{min} for various values of σ in the range from 5° to 30°, in the increments of 5°, as presented in Figure S4. The minimum of the residual error squares shows that the best fit to the experimental data is achieved for σ = 16.7° (Figure S4). On the other hand, σ is related to the curvature κ (the effective "force constant") of the free energy potential (eq 3), which shows how susceptible the ensemble is to shift under the external perturbation. By fitting the change of tilt angle as a function of the applied field (Figure 4a) to eq 7, we obtain $\kappa = (4.0 \pm 0.8) \times 10^{-20}$ J/rad^2 (or κ = 0.25 ± 0.05 eV/rad^2 , approximately 10kT per rad^2), which corresponds to $\sigma = \sqrt{\frac{k_B T}{\kappa}} \approx 0.3$ rad = 18°. These two results agree within the experimental error of ±2°. Thus, the self-consistent analysis of the field-modulated SFG spectra allows one to extract the free energy orienting potential for the free OD molecules at the water−graphene interface. It should be noted that this model assumes a simplified picture for the electric field (i.e., $-\vec{\mu}\cdot\vec{E}$). However, the presence of hydrogen bonding may impact the uniformity of the field.

There have been multiple attempts to perform MD simulations on the water/graphene system. Ostrowski et al. plot the angular distribution of $\hat{\mu}_0 \cdot \hat{z}$ under p-doped, neutral, and n-doped conditions.[45] Under n-doping conditions, a shoulder peak appears in the distribution around 53° from normal, in qualitative agreement with our observations possibly due to free OH species. However, it is not possible to determine if the free OH is changing in orientation because there are only three doping conditions explored. Nagata et al. also reported MD simulations of the D_2O/graphene system and predict a free OD feature around 2645 cm^{-1} at zero applied field.[27] However, no orientation information of the free OD was given nor its no voltage dependence. Joutsuka et al. calculated the SFG spectra of water molecules at the water/air interface under various applied electric fields.[46] They found an increase in the free OH peak intensity as the electric field becomes more negative, in agreement with our observations.

https://doi.org/10.1021/acs.jpcc.2c06063
J. Phys. Chem. C XXXX, XXX, XXX−XXX

In comparing our results with those of various theorists working in the field, there are a few notable differences.[25−27,47] Zhang et al. performed first-principles calculations of the water/graphene interface and predicted a free OH peak at zero applied voltage. In our work, however, we need to apply negative potentials to observe this free OD feature. These calculations are based on calculated water−graphene potentials that may inaccurately predict force constants and charge distributions in graphene (e.g., pooling of charge in the graphene), which are hard to reproduce in *ab initio* and DFT. Another possible reason for this discrepancy is the underlying calcium fluoride substrate, which may play a role in the interfacial fields and dipoles. Second, Zhang et al. saw an increase in the H-bonded peak intensity as a function of increasing voltage, whereas we observe a decrease and complete suppression of the H-bonded peaks, which calls into question the interpretation of surface versus bulk contributions to the measured SFG signal. Zhang et al. also calculated the distribution of OH bond angles of the topmost water layer at the electrified graphene interface and found two dominant features: (1) the free OH bond was centered around 20° from normal, much closer to normal than our observations (32°−46°) and relatively narrow in line width (20 FWHM). (2) Even under large applied potentials, they observe a majority of the OD bonds are lying in the plane of the water surface (i.e., centered around 90° from normal) and are thus hydrogen bonded. Lastly, they predict a vibrational Stark shift of the free OD peak to lower frequencies, which we do not see experimentally. This discrepancy between theory and experiment could be due to the fact that their free OH bond angles are much closer to normal and therefore feel a stronger component of the *E*-field at the electrode surface. It is likely that the detailed structure of the hydrogen bonding is playing an in important role in screening of the applied electric field. It is important to note that these simulations are performed on relatively small volumes of water (i.e., 6 nm thick). Their applied voltages of 2.5 V may correspond to electric fields that are substantially higher than those applied in our study, which could be another reason for this discrepancy.

In Figure 2, there is a substantial blue-shift of the free OD vibrational frequency, as observed in the PPP polarization configuration, while the SSP spectra remain unchanged. Naïvely, one would expect that as the average angle ($\langle\theta\rangle$) decreases, the OD bond experiences a higher field and the vibrational frequency ($\omega_{\text{free-OD}}$) should red-shift, as the bond becomes weaker due to the externally applied perturbation, consistent with the Stark effect. Instead, however, we observe a 6 cm^{-1} blue-shift of this free OD feature due to an orientational-dependent change in the hydrogen-bonding structure at this water/graphene interface. That is, as the average angle ($\langle\theta\rangle$) decreases (i.e., becomes closer to surface normal), the OD bond becomes less hydrogen bonded, resulting in a blue-shift in its vibrational frequency, that is, more like gas phase D_2O. One open question that remains is why the PPP spectra blue-shift while the SSP spectra remain constant with applied field, which we attribute to the anisotropy of the polarizability tensor associated with the interfacial water species.

CONCLUSIONS

In conclusion, we have used vibrational SFG spectroscopy to obtain the free OD bond angle with respect to surface normal from the ratio of the SFG amplitudes taken in the SSP and PPP polarization combinations as a function of applied potential. By correlating the OD orientation with the applied field, a phenomenological model of the orienting free energy potential (potential of mean force, PMF) was developed, which allows us to extract both the mean tilt angle (the location of the minimum) and the curvature (the effective force constant) near the minimum. The curvature of the PMF determines the width of the orientational distribution and also the stiffness of the potential with respect to distortion by the externally applied field. While this phenological model is based on several approximations, we obtain a value for the PMF curvature of $\kappa = (4.0 \pm 0.8) \times 10^{-20}$ J/rad^2 (or $\kappa = 0.25 \pm 0.05$ eV/rad^2). Furthermore, this basic free energy potential approach provides an analytic model of the statistical mechanics of the system, allowing one to predict equilibrium properties, fluctuations, and rates of transformations such as hydrogen bond dynamics, phase transitions, and chemical reactions.

ASSOCIATED CONTENT

Supporting Information

The Supporting Information is available free of charge at https://pubs.acs.org/doi/10.1021/acs.jpcc.2c06063.

Detailed data related to the relationship of surface electric field vs applied potentials and bonding angles; comparison of our data and theoretical calculations; a table of parameters from text; detailed description of orientational analysis and spectral fits (PDF)

AUTHOR INFORMATION

Corresponding Author

Stephen B. Cronin − *Department of Chemistry and Department of Electrical Engineering, University of Southern California, Los Angeles, California 90089, United States;* orcid.org/0000-0001-9153-7687; Email: scronin@usc.edu

Authors

Angelo Montenegro − *Department of Chemistry, University of Southern California, Los Angeles, California 90089, United States*

Ariel E. Vaughn − *Department of Chemistry, California State University, Channel Islands, Camarillo, California 93012, United States*

Muhammet Mammetkuliyev − *Department of Chemistry, University of Southern California, Los Angeles, California 90089, United States*

Bofan Zhao − *Department of Electrical Engineering, University of Southern California, Los Angeles, California 90089, United States;* orcid.org/0000-0003-0478-6330

Boxin Zhang − *Department of Electrical Engineering, University of Southern California, Los Angeles, California 90089, United States*

Haotian Shi − *Department of Electrical Engineering, University of Southern California, Los Angeles, California 90089, United States*

Dhritiman Bhattacharyya − *Department of Chemistry, University of Southern California, Los Angeles, California 90089, United States;* orcid.org/0000-0001-6761-8655

Alexander V. Benderskii − *Department of Chemistry, University of Southern California, Los Angeles, California 90089, United States;* orcid.org/0000-0001-7031-2630

https://doi.org/10.1021/acs.jpcc.2c06063
J. Phys. Chem. C XXXX, XXX, XXX−XXX

Complete contact information is available at:
https://pubs.acs.org/10.1021/acs.jpcc.2c06063

Notes

The authors declare no competing financial interest.

■ ACKNOWLEDGMENTS

This research was supported by Air Force Office of Scientific Research (AFOSR) Grants FA9550-15-1-0184 and FA9550-19-1-0115 (A.M., A.E.V., D.B., M.M., S.B.C., A.V.B.), the Army Research Office (ARO) Award Nos. W911NF1710325 (H.S.) and W911NF2210284 (B.Z.), and the National Science Foundation (NSF) Award No. CBET-2012845 (B.Z.). A.E.V. acknowledges support from the GRFP from the National Science Foundation under Grant DGE-1418060 and the National GEM Consortium with Los Alamos National Laboratory. The authors thank the Tongva people for the stewardship of the land that this research was conducted on.

■ REFERENCES

(1) Jarzynski, C. Nonequilibrium Equality for Free Energy Differences. *Phys. Rev. Lett.* **1997**, *78* (14), 2690−2693.
(2) Jarzynski, C. Equilibrium free-energy differences from non-equilibrium measurements: A master-equation approach. *Phys. Rev. E* **1997**, *56* (5), 5018−5035.
(3) Hou, B.; Laanait, N.; Yu, H.; Bu, W.; Yoon, J.; Lin, B.; Meron, M.; Luo, G.; Vanysek, P.; Schlossman, M. L. Ion Distributions at the Water/1,2-Dichloroethane Interface: Potential of Mean Force Approach to Analyzing X-ray Reflectivity and Interfacial Tension Measurements. *J. Phys. Chem. B* **2013**, *117* (17), 5365−5378.
(4) Zhang, M.; Hao, H.; Zhou, D.; Duan, Y.; Wang, Y.; Bian, H. Understanding the Microscopic Structure of a "Water-in-Salt" Lithium Ion Battery Electrolyte Probed with Ultrafast IR Spectroscopy. *J. Phys. Chem. C* **2020**, *124* (16), 8594−8604.
(5) Fayer, M. D. Dynamics of Water Interacting with Interfaces, Molecules, and Ions. *Acc. Chem. Res.* **2012**, *45* (1), 3−14.
(6) Toney, M. F.; Howard, J. N.; Richer, J.; Borges, G. L.; Gordon, J. G.; Melroy, O. R.; Wiesler, D. G.; Yee, D.; Sorensen, L. B. Voltage-dependent ordering of water molecules at an electrode−electrolyte interface. *Nature* **1994**, *368* (6470), 444−446.
(7) Singh, P. C.; Nihonyanagi, S.; Yamaguchi, S.; Tahara, T. Interfacial water in the vicinity of a positively charged interface studied by steady-state and time-resolved heterodyne-detected vibrational sum frequency generation. *J. Chem. Phys.* **2014**, *141* (18), 18C527.
(8) Dutta, C.; Svirida, A.; Mammetkuliyev, M.; Rukhadze, M.; Benderskii, A. V. Insight into Water Structure at the Surfactant Surfaces and in Microemulsion Confinement. *J. Phys. Chem. B* **2017**, *121* (31), 7447−7454.
(9) Dutta, C.; Mammetkuliyev, M.; Benderskii, A. V. Re-orientation of water molecules in response to surface charge at surfactant interfaces. *J. Chem. Phys.* **2019**, *151* (3), 034703.
(10) Singh, P. C.; Nihonyanagi, S.; Yamaguchi, S.; Tahara, T. Ultrafast vibrational dynamics of water at a charged interface revealed by two-dimensional heterodyne-detected vibrational sum frequency generation. *J. Chem. Phys.* **2012**, *137* (9), 094706.
(11) Nihonyanagi, S.; Yamaguchi, S.; Tahara, T. Direct evidence for orientational flip-flop of water molecules at charged interfaces: A heterodyne-detected vibrational sum frequency generation study. *J. Chem. Phys.* **2009**, *130* (20), 204704.
(12) Boyd, R. W.*Nonlinear Optics*; Elsevier: 2020.
(13) Du, Q.; Freysz, E.; Shen, Y. R. Vibrational spectra of water molecules at quartz/water interfaces. *Phys. Rev. Lett.* **1994**, *72* (2), 238−241.
(14) Du, Q.; Superfine, R.; Freysz, E.; Shen, Y. R. Vibrational spectroscopy of water at the vapor/water interface. *Phys. Rev. Lett.* **1993**, *70* (15), 2313−2316.
(15) Wen, Y.-C.; Zha, S.; Liu, X.; Yang, S.; Guo, P.; Shi, G.; Fang, H.; Shen, Y. R.; Tian, C. Unveiling Microscopic Structures of Charged Water Interfaces by Surface-Specific Vibrational Spectroscopy. *Phys. Rev. Lett.* **2016**, *116* (1), 016101.
(16) Ohno, P. E.; Wang, H.-f.; Geiger, F. M. Second-order spectral lineshapes from charged interfaces. *Nat. Commun.* **2017**, *8* (1), 1032.
(17) Ohno, P. E.; Wang, H.-f.; Paesani, F.; Skinner, J. L.; Geiger, F. M. Second-Order Vibrational Lineshapes from the Air/Water Interface. *J. Phys. Chem. A* **2018**, *122* (18), 4457−4464.
(18) AlSalem, H. S.; Holroyd, C.; Danial Iswan, M.; Horn, A. B.; Denecke, M. A.; Koehler, S. P. K. Characterisation, coverage, and orientation of functionalised graphene using sum-frequency generation spectroscopy. *Phys. Chem. Chem. Phys.* **2018**, *20* (13), 8962−8967.
(19) Peng, Q.; Chen, J.; Ji, H.; Morita, A.; Ye, S. Origin of the Overpotential for the Oxygen Evolution Reaction on a Well-Defined Graphene Electrode Probed by in Situ Sum Frequency Generation Vibrational Spectroscopy. *J. Am. Chem. Soc.* **2018**, *140* (46), 15568−15571.
(20) Kim, D.; Kim, E.; Park, S.; Kim, S.; Min, B. K.; Yoon, H. J.; Kwak, K.; Cho, M. Wettability of graphene and interfacial water structure. *Chem.* **2021**, *7* (6), 1602−1614.
(21) Dreier, L. B.; Nagata, Y.; Lutz, H.; Gonella, G.; Hunger, J.; Backus, E. H. G.; Bonn, M. Saturation of charge-induced water alignment at model membrane surfaces. *Sci. Adv.* **2018**, *4* (3), eaap7415.
(22) Montenegro, A.; Dutta, C.; Mammetkuliev, M.; Shi, H.; Hou, B.; Bhattacharyya, D.; Zhao, B.; Cronin, S. B.; Benderskii, A. V. Asymmetric response of interfacial water to applied electric fields. *Nature* **2021**, *594* (7861), 62−65.
(23) Vinaykin, M.; Benderskii, A. V. Vibrational Sum-Frequency Spectrum of the Water Bend at the Air/Water Interface. *J. Phys. Chem. Lett.* **2012**, *3* (22), 3348−3352.
(24) Dutta, C.; Benderskii, A. V. On the Assignment of the Vibrational Spectrum of the Water Bend at the Air/Water Interface. *J. Phys. Chem. Lett.* **2017**, *8* (4), 801−804.
(25) Zhang, Y.; de Aguiar, H. B.; Hynes, J. T.; Laage, D. Water Structure, Dynamics, and Sum-Frequency Generation Spectra at Electrified Graphene Interfaces. *J. Phys. Chem. Lett.* **2020**, *11* (3), 624−631.
(26) Zhang, Y.; Stirnemann, G.; Hynes, J. T.; Laage, D. Water dynamics at electrified graphene interfaces: a jump model perspective. *Phys. Chem. Chem. Phys.* **2020**, *22* (19), 10581−10591.
(27) Ohto, T.; Tada, H.; Nagata, Y. Structure and dynamics of water at water−graphene and water−hexagonal boron-nitride sheet interfaces revealed by ab initio sum-frequency generation spectroscopy. *Phys. Chem. Chem. Phys.* **2018**, *20* (18), 12979−12985.
(28) Ostrowski, J. H. J.; Eaves, J. D. The Tunable Hydrophobic Effect on Electrically Doped Graphene. *J. Phys. Chem. B* **2014**, *118* (2), 530−536.
(29) Shi, H.; Poudel, N.; Hou, B.; Shen, L.; Chen, J.; Benderskii, A. V.; Cronin, S. B. Sensing local pH and ion concentration at graphene electrode surfaces using in situ Raman spectroscopy. *Nanoscale* **2018**, *10* (5), 2398−2403.
(30) Shi, H.; Zhao, B.; Ma, J.; Bronson, M. J., Jr.; Cai, Z.; Chen, J.; Wang, Y.; Cronin, M.; Jensen, L.; Cronin, S. B. Measuring Local Electric Fields and Local Charge Densities at Electrode Surfaces Using Graphene-Enhanced Raman Spectroscopy (GERS)-Based Stark-Shifts. *ACS Appl. Mater. Interfaces* **2019**, *11* (39), 36252−36258.
(31) Chae, H. U.; Ahsan, R.; Tao, J.; Cronin, S. B.; Kapadia, R. Tunable Onset of Hydrogen Evolution in Graphene with Hot Electrons. *Nano Lett.* **2020**, *20* (3), 1791−1799.
(32) Vaughn, A. E.; Montenegro, A.; Howard, E. S.; Mammetkuliyev, M.; Falcon, S.; Mecklenburg, M.; Melot, B. C.; Benderskii, A. V. Vibrational Sum Frequency Generation Spectroscopy of Surface Hydroxyls on Nickel Phyllosilicate Nanoscrolls. *J. Phys. Chem. Lett.* **2021**, *12*, 10366.

(33) Das Sarma, S.; Adam, S.; Hwang, E. H.; Rossi, E. Electronic transport in two-dimensional graphene. *Rev. Mod. Phys.* **2011**, *83* (2), 407−470.
(34) Froehlicher, G.; Berciaud, S. Raman spectroscopy of electrochemically gated graphene transistors: Geometrical capacitance, electron-phonon, electron-electron, and electron-defect scattering. *Phys. Rev. B* **2015**, *91* (20), 205413.
(35) Stiopkin, I. V.; Weeraman, C.; Pieniazek, P. A.; Shalhout, F. Y.; Skinner, J. L.; Benderskii, A. V. Hydrogen bonding at the water surface revealed by isotopic dilution spectroscopy. *Nature* **2011**, *474* (7350), 192−195.
(36) Gan, W.; Wu, D.; Zhang, Z.; Guo, Y.; Wang, H.-f. Orientation and Motion of Water Molecules at Air/Water Interface. *Chinese Journal of Chemical Physics* **2006**, *19* (1), 20−24.
(37) Auer, B.; Kumar, R.; Schmidt, J. R.; Skinner, J. L. Hydrogen bonding and Raman, IR, and 2D-IR spectroscopy of dilute HOD in liquid D_2O. *Proc. Natl. Acad. Sci. U. S. A.* **2007**, *104* (36), 14215.
(38) Wang, H.; Gan, W.; Lu, R.; Rao, Y.; Wu, B. Quantitative spectral and orientational analysis in surface sum frequency generation vibrational spectroscopy (SFG-VS). *Int. Rev. Phys. Chem.* **2005**, *24* (2), 191−256.
(39) Akamatsu, N.; Domen, K.; Hirose, C. SFG study of two-dimensional orientation of surface methyl groups on cadmium arachidate Langmuir-Blodgett films. *J. Phys. Chem.* **1993**, *97* (39), 10070−10075.
(40) Zhuang, X.; Miranda, P. B.; Kim, D.; Shen, Y. R. Mapping molecular orientation and conformation at interfaces by surface nonlinear optics. *Phys. Rev. B* **1999**, *59* (19), 12632−12640.
(41) Avila, G.; Fernández, J. M.; Tejeda, G.; Montero, S. The Raman spectra and cross-sections of H_2O, D_2O, and HDO in the OH/OD stretching regions. *J. Mol. Spectrosc.* **2004**, *228* (1), 38−65.
(42) Sun, S.; Tang, F.; Imoto, S.; Moberg, D. R.; Ohto, T.; Paesani, F.; Bonn, M.; Backus, E. H. G.; Nagata, Y. Orientational Distribution of Free O-H Groups of Interfacial Water is Exponential. *Phys. Rev. Lett.* **2018**, *121* (24), 246101.
(43) de Beer, A. G. F.; Roke, S. What interactions can distort the orientational distribution of interfacial water molecules as probed by second harmonic and sum frequency generation? *J. Chem. Phys.* **2016**, *145* (4), 044705.
(44) Gan, W.; Feng, R.-R.; Wang, H.-F. Comment on "Orientational Distribution of Free O-H Groups of Interfacial Water is Exponential". *Phys. Rev. Lett.* **2019**, *123* (9), 099601.
(45) Ostrowski, J. H. J.; Eaves, J. D. The Tunable Hydrophobic Effect on Electrically Doped Graphene. *J. Phys. Chem. B* **2014**, *118*, 530.
(46) Joutsuka, T.; Hirano, T.; Sprik, M.; Morita, A. Effects of third-order susceptibility in sum frequency generation spectra: a molecular dynamics study in liquid water. *Phys. Chem. Chem. Phys.* **2018**, *20* (5), 3040−3053.
(47) Sun, S. M.; Tang, F. J.; Imoto, S.; Moberg, D. R.; Ohto, T.; Paesani, F.; Bonn, M.; Backus, E. H. G.; Nagata, Y. Orientational Distribution of Free O-H Groups of Interfacial Water is Exponential. *Phys. Rev. Lett.* **2018**, *121* (24), 246101.

https://doi.org/10.1021/acs.jpcc.2c06063
J. Phys. Chem. C XXXX, XXX, XXX−XXX